Design study of a combined interferometer and polarimeter for a high-field, compact tokamak

Physics of Plasmas ARTICLE scitation.org/journal/php

Design study of a combined interferometer and polarimeter for a high-field, compact tokamak

Cite as: Phys. Plasmas **27**, 042516 (2020); doi: 10.1063/1.5142638
Submitted: 19 December 2019 · Accepted: 31 March 2020 ·
Published Online: 23 April 2020

Alexander J. Creely, Lucio M. Milanese,[a] Elizabeth A. Tolman, James H. Irby, Sean B. Ballinger, Samuel Frank, Adam Q. Kuang, Bryan L. Linehan, William McCarthy, Kevin J. Montes, Theodore Mouratidis, Julian F. Picard, Pablo Rodriguez-Fernandez, Aaron M. Rosenthal, Alexander J. Sandberg, Francesco Sciortino, Raspberry A. Simpson, R. Alexander Tinguely, Muni Zhou, and Anne E. White

AFFILIATIONS

Massachusetts Institute of Technology, Plasma Science and Fusion Center, 77 Massachusetts Ave., Cambridge, Massachusetts 02139, USA

[a]Author to whom correspondence should be addressed: milanese@mit.edu

ABSTRACT

This article is the first design study of a combined interferometer and polarimeter on a compact, high-field, high-density, net-energy tokamak. Recent advances in superconducting technology have made possible designs for compact, high magnetic field fusion power plants, such as ARC [Sorbom *et al.*, Fusion Eng. Des. **100**, 378 (2015)], and experiments, such as SPARC [Greenwald *et al.*, PSFC Report No. RR-18-2 (2018)]. These new designs create both challenges and opportunities for plasma diagnostics. The diagnostic proposed in this work, called InterPol, takes advantage of unique opportunities provided by high magnetic field and density to measure both line-averaged density and poloidal magnetic field with a single set of CO_2 and quantum cascade lasers. These measurements will be used for fast density feedback control, constraint of density and safety factor profiles, and density fluctuation measurements. Synthetic diagnostic testing using a model machine geometry, called MQ1 (Mission Q $\geq$ 1), and profiles simulated with Tokamak Simulation Code indicate that InterPol will be able to measure steady state density and poloidal magnetic field, as well as fluctuations caused by toroidal Alfvén eigenmodes and other phenomena on a high-field compact tokamak.

I. INTRODUCTION

Next-generation fusion experiments will investigate ways to reduce the size, cost, and complexity of an eventual fusion power plant. To achieve the necessary performance at a small size, a power plant will want to maximize its volumetric fusion power density P_f/V_p, which is governed by the relationship[1]

$$\frac{P_f}{V_p} \propto \langle p \rangle^2 \propto \beta_T^2 B_0^4, \tag{1}$$

where P_f is the fusion power, V_p is the plasma volume, $\langle p \rangle$ is the volume-averaged plasma pressure, B_0 is the toroidal magnetic field, and $\beta_T \equiv 2\mu_0 \langle p \rangle / B_0^2$ is the toroidal plasma beta. In this relationship, β_T is limited by magnetohydrodynamic stability,[2] while B_0 is limited by materials and engineering constraints. Thus, one can improve the volumetric power density by pursuing advanced physics operation (increasing β_T) or by pursuing advanced engineering options (increasing B_0).

Until recently, the maximum on-axis magnetic field achievable in a tokamak with superconducting magnets has been limited by material properties to roughly 6 T.[3] ITER's on-axis field of $B_0 = 5.3$ T is partly a result of these limitations.[4] The recent development and commercialization of high temperature superconductors (HTS) allow on-axis fields of up to 12 T, resulting in designs for machines such as ARC[5] and the recently proposed SPARC.[6–9] Both of these machines utilize high magnetic fields to produce large amounts of fusion energy in machines much smaller than ITER, and more comparable in size to present-day tokamaks.

High-field, compact tokamak concepts will operate in a different parameter space than present-day machines; in addition to being smaller and of higher magnetic field, these machines will also likely have higher plasma and current densities. These differences present both challenges and opportunities for diagnostics. This work describes a combined two-color interferometer and polarimeter, known as InterPol, which addresses these challenges and opportunities. A complementary suite of neutron diagnostics for a high-field tokamak is presented in Ref. 10.

This paper begins by outlining the operational principles of interferometry and polarimetry in Sec. II. Section III then uses a model high-field tokamak, called MQ1 (Mission Q $\geq$ 1), based on a proposal in Ref. 3 with parameters similar to those proposed for SPARC, to explore the ways in which high magnetic field, density, and current impact the operation of interferometry and polarimetry. Based on this information, Sec. IV describes the proposed design for InterPol on MQ1. Finally, Sec. V utilizes the model machine geometry and synthetic diagnostics to predict signal levels.

II. INTERFEROMETRY AND POLARIMETRY

Interferometry is used to measure tokamak plasma density, while polarimetry is used to measure the product of density and magnetic field parallel to the direction of propagation of the beam.[11] In this section, the physical principles underlying these diagnostics are reviewed.

Interferometry uses the fact that a beam of light traveling through a plasma will experience a phase delay with respect to an equivalent beam that has traveled through a vacuum. To first order in $T_e/(m_e c^2)$, this phase delay is given by[11,12]

$$\Delta\phi = \frac{-e^2\lambda}{4\pi c^2 m_e \epsilon_0}\int n_e\left[1-\frac{3}{2}\frac{T_e}{m_e c^2}\right]dl, \tag{2}$$

where $\Delta\phi$ is the phase delay experienced by the interferometer, e is the fundamental charge, λ is the wavelength of the light, c is the speed of light, m_e is the electron mass, ϵ_0 is the permittivity of free space, n_e is the local electron density, T_e is the local electron temperature, and dl is the path length along which the laser travels. In present-day tokamaks, the temperature term in Eq. (2) is often negligible, such that the phase delay can be straightforwardly used to calculate line-integrated density. As will be described later, it is possible to use a combined interferometer–polarimeter to account for these finite temperature effects, without relying on a separate diagnostic for temperature measurements.

Interferometry is very robust and can measure plasma density with fast enough time resolution and automated analysis (much faster than the confinement time) to allow for active feedback control of the plasma density.[13] In addition, one can use multiple chords in order to invert a density profile in the plasma. These measurements are vital to machine operation and optimization of plasma performance.

Polarimetry uses the fact that a linearly polarized wave traveling through a plasma parallel to a magnetic field will experience a rotation of its polarization, known as Faraday rotation.[11] This allows the following statement:[11,12]

$$\alpha = \frac{e^3\lambda^2}{8\pi^2 m_e^2 c^3 \epsilon_0}\int n_e\left[1-2\frac{T_e}{m_e c^2}\right]\vec{B}\cdot\vec{dl}, \tag{3}$$

where α is the angle of Faraday rotation (half of the angle by which the linear polarization rotates), $\vec{B}$ is the magnetic field, and $\vec{dl}$ is the path length vector of the laser as it travels through the plasma. Again, in present-day tokamaks, the temperature term in Eq. (3) is usually negligible, such that polarimetry directly measures the combination of the electron density and the parallel magnetic field along the chord. One can measure the density utilizing the results of the interferometer and thus calculate the magnetic field parallel to the beam chord. Polarimetry allows the calculation of current and safety factor profiles, which are both important for stability against disruptions and optimizing the performance of future steady state machines.[14]

In addition, both diagnostics can measure plasma fluctuations (in density and magnetic field, respectively), which are important to understanding tokamak transport and to the validation of turbulent transport models.[15,16]

III. OPPORTUNITIES AND CHALLENGES OF HIGH-FIELD INTERFEROMETRY AND POLARIMETRY

Compact, high-magnetic field devices present both opportunities and challenges for interferometry and polarimetry diagnostics. Such devices will operate at higher temperatures than most present devices and higher plasma and current densities than both current devices and ITER. To illustrate these tradeoffs concretely, this paper evaluates InterPol's diagnostic capabilities on a conceptual design of a compact, high-field tokamak, which will be referred to as MQ1.[3] This machine has a major radius of 1.65 m and a minor radius of 0.5 m (roughly the size of DIII-D or ASDEX Upgrade). The toroidal field on axis is 12 T and the flattop plasma current is 7.5 MA. This machine can be thought of as a smaller prototype for a high-field power plant, such as the ARC tokamak,[5] and has parameters similar to those which might be used in the SPARC device. Table I lays out many of the most important parameters associated with MQ1.

To obtain information necessary for a conceptual design study, the MQ1 tokamak was simulated using the time-dependent Grad–Shafranov solver, TSC (Tokamak Simulation Code).[17] Density and temperature profiles are estimated within the TSC using the highly simplified Coppi–Tang model;[18,19] the H-mode condition is approximated by artificially reducing the transport over a narrow edge region.

Figure 1 shows the magnetic equilibrium from the TSC during the flattop portion of the MQ1 discharge. Figure 2 shows one dimensional ion and electron temperature and electron density profiles, also from the flattop portion of the MQ1 discharge. These profiles are associated with the parameters given in Table I. Note that these profiles are only meant to be realistic enough to investigate the use of InterPol, not to exactly represent the profiles in a future machine. The machine is also assumed to operate with a 50–50 mix of deuterium and tritium, and an effective charge $Z_{eff} \approx 1.2$.

MQ1's plasma temperature is much higher than typical temperatures in present-day tokamaks. This means that the temperature terms

TABLE I. MQ1 tokamak machine and plasma parameters.[3]

Parameter	Value
Major radius (R)	1.65 m
Minor radius (a)	0.5 m
On-axis toroidal field (B_0)	12 T
Plasma current (I_p)	7.5 MA
Elongation (κ)	1.8
Plasma triangularity (δ)	0.4
95% flux surface safety factor (q_{95})	3.0
On-axis electron density ($n_{e,0}$)	4.0×10^{20} m^{-3}
On-axis electron temperature ($T_{e,0}$)	22 keV
External heating power (P_{ext})	30 MW
Fusion power (P_{fusion})	100 MW
Fusion gain (Q)	3.3

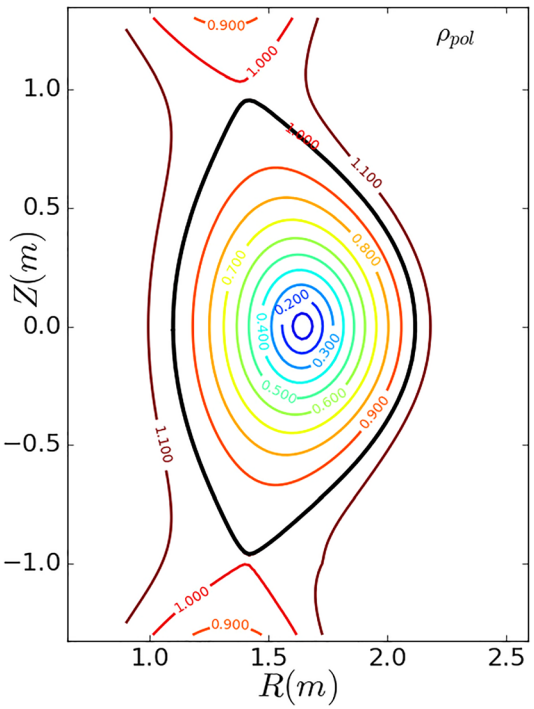

FIG. 1. Magnetic equilibrium of the MQ1 model tokamak during flattop operation. Contours are of ρ_{pol}, which is defined as the square root of the normalized poloidal magnetic flux. Equilibrium taken from the TSC output.

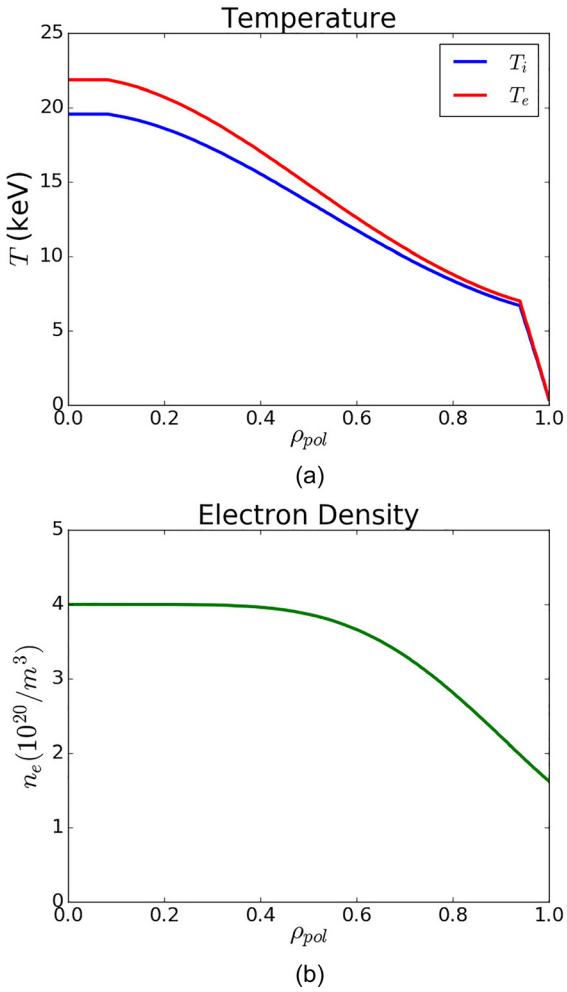

FIG. 2. Model ion (blue) and electron (red) temperature (a) and electron density (b) profiles for MQ1 during flattop operation, as predicted by the Coppi–Tang model used within the TSC.

in Eqs. (2) and (3) are not negligible, a challenge that MQ1 shares with lower-field devices like ITER. Like ITER, MQ1 can address this challenge by combining interferometry and polarimetry measurements to correct for the finite temperature effects to first order, without using measurements from a separate temperature diagnostic. While the details of these calculations will not be repeated here, they can be found in Refs. 12 and 20. Second order effects lead to changes of order 0.1%, which is much less than the instrumental uncertainty for polarimetry measurements and similar to the instrumental uncertainty for interferometry measurements. Second order effects can be accounted for, with relatively large uncertainty, via estimates of chord-averaged temperature profiles obtained from other diagnostics or the combination of interferometry and polarimetry measurements.

Since both interferometry and polarimetry signals are proportional to line-integrated density and polarimetry is proportional to poloidal magnetic field, which depends on current density [see Eqs. (2) and (3)], higher plasma and current density increase the signal magnitude of both measurements. This creates an opportunity to use shorter wavelengths for measurements, for which more reliable sources exist. The design proposed here makes use of a single set of CO_2 and quantum cascade lasers (QCL) for both (two color) interferometry and polarimetry. This will be discussed in greater detail in Sec. IV.

A compact size, however, also leads to challenges, such as high neutron fluxes outside of the machine and high heat fluxes on the divertor. The neutron flux means that shielding of neutron-sensitive components is more important. High divertor heat flux means that it may be advantageous for the machine to operate in a balanced double null configuration with toroidally continuous divertors, which would prevent vertical lines of sight that would otherwise be possible. This work therefore proposes a diagnostic that does not include vertical lines of sight.

The MQ1 parameters and profiles presented in this section will be used to investigate what a combined interferometer–polarimeter will look like on a compact, high-field fusion experiment like MQ1.

IV. PROPOSED INTERPOL DIAGNOSTIC

This section presents the proposal for InterPol on MQ1, which addresses the challenges and opportunities presented in Sec. III, starting with consideration of diagnostic geometry. Many existing tokamaks, including Alcator C-Mod[13] and EAST,[21] utilize a series of parallel beams. Parallel beams can simplify engineering and make the inversion of interferometer data (to obtain radial profiles) more straightforward. However, these designs require many penetrations in

the first wall, which is problematic in the high-neutron flux environment of a compact, high-field tokamak.

To minimize first wall penetrations and thus allow better neutron shielding, especially of the detectors and other electronic components required to operate the interferometer and polarimeter, InterPol proposes a geometry with a single first wall penetration on the low-field side midplane, similar to the poloidal polarimeter design on ITER.[22] The beams will reflect on the high-field side off of retroreflectors and then pass again through the first wall (retroreflectors will be discussed in more detail later in this section). Figure 3 shows the geometry for InterPol overlaid on contours of density obtained from mapping the one-dimensional profiles from the TSC onto the two-dimensional equilibrium given in Fig. 1. Density is given in units of $10^{20}/\mathrm{m}^3$. The red lines are the proposed chords for the InterPol system.

The system consists of 11 chords in a poloidal plane, originating at the outboard midplane and propagating inward at angles of 0°, 7°, 14°, 21°, ±27°, 32°, 37°, 41°, and ±45°. This angular spacing means that the chords are evenly spaced in slope and thus are evenly spaced in Z at any given radius. These chord angles are chosen to roughly cover the extent of the plasma evenly without requiring retroreflectors to be placed in the divertor regions of the machine. The asymmetric arrangement was chosen to offer high radial resolution over part of the plasma, without requiring a large number of chords. This design will operate most effectively in an up-down symmetric plasma. We underline that the exact location of the retroreflectors and, thus, the angle of the chords would be subject to a further optimization based on more detailed profiles in expected scenarios and engineering constrains of the MQ1 machine.

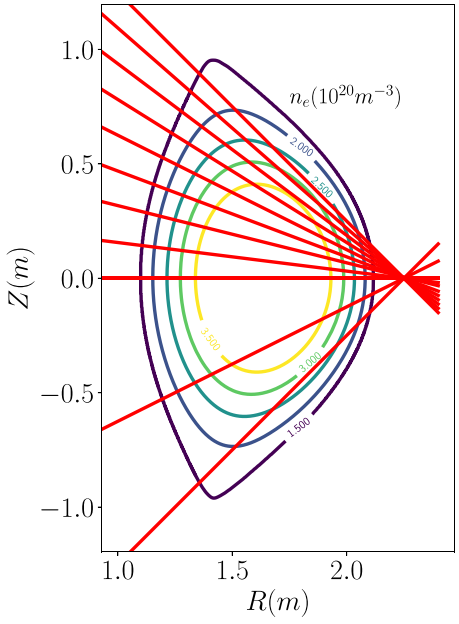

FIG. 3. Proposed chord geometry for the InterPol diagnostic on MQ1. An asymmetric chord arrangement gives greater maximum spatial resolution but works best when the plasma is up-down symmetric. Red lines indicate the laser chords. Contours are of plasma density in units of $10^{20}/\mathrm{m}^3$.

TABLE II. Average relative error on reconstructured density profile as function of the steepness of the density profile [parameterized by ν in Eq. (4)] and the number of chords in the upper midplane (N).

ν \ N	6	7	8	9
0.20	3.1%	2.9%	2.6%	2.6%
0.30	4.7%	4.3%	3.9%	3.7%
0.35	5.6%	5.0%	4.6%	4.4%
0.4	6.3%	5.8%	5.3%	4.9%

We investigated the accuracy of the profile obtained from Abel inversion as a function of the number of chords in the upper midplane and the steepness of the density profile. We used a synthetic diagnostic on a density profile modeled analytically[23] as

$$n(\rho_{pol}) = n_0(1-\rho_{pol}^2)^{\nu}. \tag{4}$$

We assumed that, when sweeping the ν parameter, the temperature profile would vary in such a way as to leave the pressure profile unchanged. The synthetic diagnostic integrates the 2D density profile over the line-of-sight of the chords and then performs Abel inversion to reconstruct a 1D density profile. The reconstructed density profile was then compared with the analytical expression in Eq. (4) and the average relative error was computed. Results are summarized in Table II. It is generally harder to perform Abel inversion accurately on steeper profiles, and the relative error is larger in the outer regions of the plasma where the density is lower. However, sweeping the upper midplane with 9 chords allows us to obtain good radial resolution and at the same time achieve an averaged relative error smaller than 5.0% even for $\nu = 0.4$, which describes a plasma density profile significantly steeper than in typical experimental conditions. The results from the synthetic diagnostic analysis presented in this section do not take into account the corrections due to the finite temperature profile when computing line-integrated quantities. As shown in Refs. 12 and 20, it is possible to take into account corrections to first order by combining interferometry and polarimetry measurements. Second-order corrections $\sim(T_e/m_ec^2)^2$ would lead to an error of order 0.1%, which is negligible given the uncertainty level from other sources of error.

Figure 4 shows the profile obtained from the TSC and the Abel-inverted reconstructed profile obtained using the synthetic diagnostic with nine chords in the upper midplane. The algorithm at the base of Abel inversion as employed in this work is described in Ref. 11. The profile obtained from the TSC does not follow the analytical expression given in Eq. (4). It is possible, however, to fit the analytical expression in Eq. (4) to the TSC profile and extract a value for the fitted parameter ν. The best fit for this parameter is $\nu = 0.36$, which is within the range for which accuracy better than 5% can be obtained for Abel-inverted profiles.

Similarly, Fig. 5 shows the poloidal field profile and its reconstruction obtained via Abel inversion from the synthetic InterPol diagnostic with nine chords. Significantly larger uncertainty exists for the poloidal field inversion than for the density inversion since the uncertainty on the polarimetry measurements is larger. Table III presents the average error on the Abel-inverted TSC profile as a function of the number of chords in the upper midplane. No full parameterization study of the B_p profile has been performed as we envision a complete

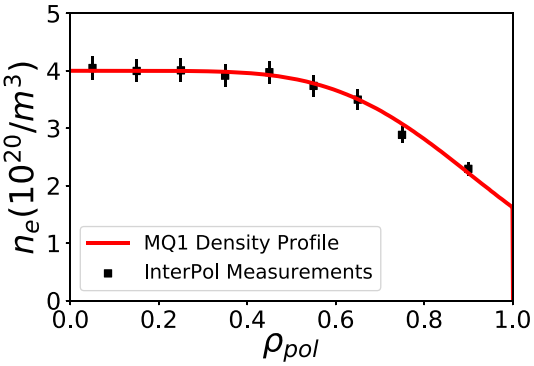

FIG. 4. Comparison between the MQ1 density profile from the TSC and Abel-inverted discrete profile obtained with the chord arrangement proposed for InterPol. Uncertainty is represented as the vertical bars.

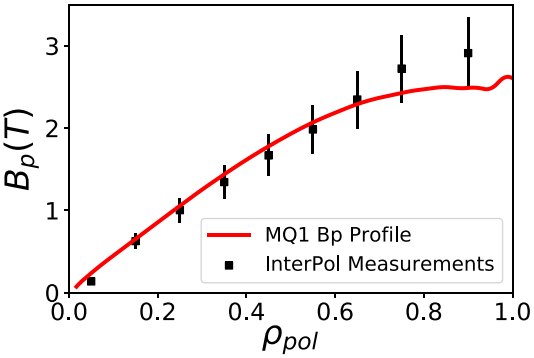

FIG. 5. Comparison between the MQ1 poloidal field profile from TSC and Abel-inverted discrete profile obtained with the chord arrangement proposed for InterPol. Uncertainty is represented as the vertical bars.

optimization of InterPol's magnetic field measurement capabilities to be undertaken in combination with other diagnostics focused on measurements of the magnetic field. (Here, B_p refers to the poloidal component of the overall magnetic field $\vec{B}$; InterPol is sensitive to this component of the magnetic field because of its chord geometry.) Overall accuracy goals on the measurements of the profiles of B_p and safety factor q should be set and optimized for based on integrated synthetic modeling of a complete diagnostic suite.

While the exact shape of the first wall of a high magnetic field machine like MQ1 is not certain, it is assumed that retroreflectors can be placed in the first wall on the high-field side of the machine, allowing both the incoming and outgoing laser beams to pass through the first wall on the low field side of the machine. The retroreflectors must be indented into a shielding layer to minimize the direct exposure to neutron flux. Sputtering damage on the retroreflectors would produce surface roughness, which can in turn reduce the reflectivity and introduce spurious changes in the polarization angle. Reference 24 presents a detailed study of the sputtering-induced damage for retroreflectors in ITER. That study calculated an upper limit of 5 μm and 1 μm sputtering-induced surface roughness on molybdenum and tungsten retroreflectors, respectively, for the lifetime operation of ITER. However, sputtering damage would be reduced by about two orders of magnitude in MQ1 compared to ITER due to the much shorter total operation time.[10,25] Thus, for both molybdenum and tungsten retroreflectors, we consider an upper limit of 0.1 μm on the level of surface roughness. This roughness level would lead to a decline in surface reflectivity smaller than 10%.[24] Moreover, as detailed in the following paragraph, placing an array of parallel retroreflectors would allow mitigating any exceptional level of damage on one of more of the components.

TABLE III. Average relative error on the reconstructured TSC B_p profile (as in Fig. 5) as a function of the number of chords in the upper midplane (N).

N	6	7	8	9
Error	11.5%	11.1%	10.9%	10.6%

If retroreflectors become severely damaged during operation, they would need to be replaced. A potential alternative is to introduce an array of several retroreflectors at each location in the inner wall, with the individual retroreflectors placed parallel to each other and controlled via hydraulic pumps. If the first retroreflector in the array gets damaged, it would be possible to use another one in the array, thus avoiding the need to replace individual retroreflectors and allowing continuous operation over several experimental campaigns.

One must select the laser wavelength for the InterPol system carefully in order to balance several competing effects. First, increasing the wavelength increases signal level for both interferometry and polarimetry, since the phase delay for interferometry is proportional to λ [see Eq. (2)] and the Faraday rotation angle for polarimetry is proportional to λ^2 [see Eq. (3)]. In addition, the impact of mechanical vibrations is more detrimental at shorter wavelengths, as the induced noise depends on the ratio of the path length change to the laser wavelength. One must also consider the Cotton–Mouton effect, proportional to λ^3, which results in a linearly polarized wave becoming elliptically polarized and can complicate polarimetry measurements[11] (longer wavelengths result in more complications). Refraction of the beam through the plasma also gets worse with longer wavelengths. Finally, reliable lasers are only available at certain wavelengths, and reliability is a key feature of a diagnostic so essential to the operation of a tokamak.

This design proposes to use 10.6 μm wavelength CO_2 lasers for the primary interferometry and polarimetry measurements and 5.22 μm QCLs for vibration correction in a setup known as compensated two-color interferometry (TCI).[13,20,26–29] The CO_2 laser technology is mature[30] and state-of-the-art quantum cascade lasers demonstrated robustness and stable performance.[20] The CO_2 laser will be primarily sensitive to the plasma, but will also be influenced by mechanical vibration. The QCL can be used to correct for the phase delay of the CO_2 caused by mechanical vibration, resulting in a signal representing only the plasma-induced phase delay. Phase measurements of both lasers can be made using a demodulator based on an FPGA (field-programmable gate array) interfaced with multiple high-frequency analog to digital converters. This system could be similar in many ways to the digital phase demodulator system described in Ref. 20. Mathematically, the relationship reads

$$\int n_e \left[1 - \frac{3}{2}\frac{T_e}{m_e c^2}\right] dl = \frac{4\pi c^2 m_e \epsilon_0}{e^2} \frac{\Delta\phi_{\mathrm{QCL}}\lambda_{\mathrm{QCL}} - \Delta\phi_{\mathrm{CO_2}}\lambda_{\mathrm{CO_2}}}{\lambda^2_{\mathrm{CO_2}} - \lambda^2_{\mathrm{QCL}}}. \quad (5)$$

Most machines, however, use longer wavelength lasers, such as $\lambda = 119\,\mu$m far infrared (FIR) CH_3OH lasers on the large helical device (LHD)[31] and $\lambda = 195\,\mu$m deuterium cyanide (DCN) lasers on ASDEX Upgrade and JET.[32–34] This is generally due to the lower plasma densities on many machines, and thus the desire to increase the signal level by increasing the wavelength. Due to the very high density expected on a device like MQ1, it would be possible to use a setup based on CO_2 and QCL, as will be described quantitatively in Sec. V. One advantage of using CO_2 lasers is their excellent reliability. On ITER, for example, it is expected that the CO_2 lasers will fail in less than one discharge per year[30] (the ITER system will be discussed in further detail below).

Intermediate wavelengths ($\sim$50 μm) would potentially allow more accurate measurements while keeping the Cotton–Mouton effect and refraction at acceptable levels (these effects will be discussed below). Some efforts have been devoted to the development of a two-color interferometer–polarimeter based on CH_3OD laser sources with $\lambda = 57.2\,\mu$m and 47.7 μm.[35,36] At present, however, this technology is immature compared to CO_2 lasers, whose reliability and robustness constitute a decisive advantage.

For the polarimetry portion of the measurement, the choice of wavelength is more constrained due to the λ^2 dependence of the Faraday rotation angle. For this reason, almost all other machines use wavelengths larger than 100 μm for poloidal polarimetry measurements. For example, ASDEX Upgrade uses the same $\lambda = 195\,\mu$m deuterium cyanide (DCN) lasers for both interferometry and polarimetry,[32,33] and both EAST and J-TEXT use $\lambda = 432.5\,\mu$m formic acid (HCOOH) FIR lasers for their combined polarimeter-interferometers (POINT on EAST[21] and POLARIS on J-TEXT[37]).

Tangentially viewing polarimeters, which do not measure poloidal magnetic field, are an exception. Since the polarimeter is sensitive to the magnetic field parallel to the direction of propagation of the beam, a tangential line of sight is sensitive primarily to the toroidal magnetic field. Combined with a longer chord length, sensitivity to the stronger toroidal magnetic field, rather than the weaker poloidal magnetic field, means that tangential interferometer–polarimeters (TIP) will have a much larger signal level than an equivalent poloidally viewing system. Thus, the tangential interferometer–polarimeter on DIII-D[38] is able to use 10.6 μm CO_2 lasers despite the relatively low density and poloidal magnetic fields of this machine. The proposed ITER tangential interferometer–polarimeter (TIP)[20,22] is also planning on using CO_2 lasers. These systems, however, do not measure the poloidal magnetic field, which is one of the main motivations of the polarimetry diagnostic. The measurement of the Faraday rotation is instead used as a second measure of the line-averaged density, since the toroidal magnetic field is well known.

MQ1's higher density and poloidal magnetic field allow the novel use of a 10.6 μm CO_2 laser for both interferometry and *poloidal* polarimetry measurements. The expected signal levels on MQ1 will be quantified in Sec. V.

While polarimetry cannot account for vibration using a second wavelength in the same way that interferometry can, various methods exist that minimize the effect of mechanical vibrations on the polarimeter signal. For example, using the signal from a detector that measures the beam phase before it passes through the plasma as the local oscillator signal, as opposed to using a separately generated local oscillator signal, significantly reduces the vibration-induced error in polarimetry.[20,22] One can also minimize the mechanical vibrations themselves by carefully designing and placing the optical components.[21]

V. PREDICTED SIGNALS AND MEASUREMENT CAPABILITIES

In order to estimate the expected signal levels of InterPol on MQ1, and thus determine if the diagnostic will be able to make useful measurements in a compact, high-field, high-density tokamak, a synthetic diagnostic was applied to the proposed MQ1 profiles. This analysis used the 2D density profile and diagnostic lines of sight shown in Fig. 3, as well as the 2D poloidal magnetic field profile from the proposed MQ1 magnetic equilibrium.

A. Steady state measurements

The predicted interferometer phase shift was evaluated by line-integrating the density along the chosen lines of sight. This line-integrated density was then inserted into Eq. (2) in order to calculate the total interferometer phase shift.

The electron temperature term in Eq. (5) has been neglected in the line-integration procedure performed here, but it can be accurately accounted for by combining the interferometry and polarimetry measurements as shown in Refs. 12 and 20.

Similarly, the anticipated Faraday rotation was calculated by integrating the plasma density times the poloidal magnetic field dotted with the chord path, and inserting the result into Eq. (3). The results of these calculations for two-pass operation (after the beam has reflected off of a retroreflector) are shown in Table IV for a subset of the system chords.

To put these signal levels into context, it is possible to obtain instrumental resolution as small as $\Delta(\Delta\phi) = 1.5°$ for the interferometry measurement and as small as $\Delta\alpha = 0.06°$ for the polarimetry measurements.[20] For the flattop plasma parameters in Table IV, this corresponds to an accuracy floor between 0.1% and 0.2% for the interferometry measurements and between 4% and 8% for the polarimetry measurements. Given the InterPol chord geometry, standard inversion calculations are able to reconstruct density profiles and to constrain inverted q-profiles for the MQ1 plasma with these signal levels.

TABLE IV. Predicted InterPol signal levels during flattop operation of MQ1. The expected interferometer two-pass phase shift and polarimeter two-pass Faraday rotation angle are calculated for the upper chords of InterPol.

Chord angle (°)	Interferometer phase shift $\Delta\phi$ (°)	Polarimeter Faraday rotation α (°)
Center (0)	1166	0.00
7	1162	0.39
14	1150	0.75
21	1128	1.06
27	1091	1.29
32	1038	1.42
37	972	1.46
41	900	1.43
45	824	1.36

Note that earlier in the discharge, when the density and plasma current (and thus poloidal field) are lower, the expected signal levels will be lower, as shown in Table V, and thus, the relative error will be larger. This relative error may be as much as 10% for interferometry and 100% for polarimetry very early in the current ramp (when the total plasma current is less than 1 MA and the plasma volume is smaller). Later in the current ramp and during the flattop, however, the signal levels are far above the instrumental sensitivity limits, suggesting that the diagnostic will be able to make high-quality measurements in this plasma.

The issue of fringe jumps in the interferometer signal, which can complicate the interpretation of interferometry measurements,[11] can be resolved using heterodyne detection and the polarimeter measurement as a reference. In particular, since the InterPol Faraday rotation angle on MQ1 is always smaller than π, this signal can be used as a reference to correct for ambiguity in the number of full 2π rotations of the interferometer phase angle after a temporary loss of signal or other issues.

Due to the very short wavelength of the CO_2 lasers, complications related to refraction and the Cotton–Mouton effect are not significant for the proposed system. Ray tracing calculations reveal that refraction will cause the beams to deviate from a straight line by less than 0.1°, which is comparable to or less than the possible alignment accuracy and vibration effects, and is therefore a negligible effect. Similarly, the ellipticity introduced by the Cotton–Mouton effect is estimated to be less than 10^{-3}, which is again negligible.

B. Fluctuation measurements

In addition to its function as a steady state diagnostic that enables density feedback control and constraint of the plasma q-profile, InterPol will also be able to function as a fluctuation diagnostic. Fluctuation measurements will, however, depend more strongly on the precision and spatial and temporal resolution of the diagnostic, so more information on these aspects of the diagnostic will be given here.

Consider first the expected noise levels in the diagnostic. These noise levels can be different from the instrumental resolution discussed above. A similar CO_2 laser-based diagnostic found that for $f > 20$ kHz, the noise levels for both interferometry and polarimetry were approximately $[10^{-6} - 10^{-5}]^{\circ 2}$/kHz, implying that for a mode that is roughly 1 kHz in width, the minimum measurable phase shift or Faraday rotation is of order $10^{-3^\circ} - 10^{-2^\circ}$.[22] Below 5 kHz, vibration and other effects limit the ability to perform fluctuation measurements. For the signal levels given above, this corresponds to a noise level of $\delta\bar{n}_e/\bar{n}_e \sim 10^{-5} - 10^{-6}$ for the interferometer and $\delta\bar{B}/\bar{B} \sim 10^{-2} - 10^{-3}$ for the polarimeter. Based on experience with current machines, these noise levels will allow for precise measurement of density fluctuations from a variety of sources (MHD, turbulence, etc.) and marginal measurement of magnetic field fluctuations.[22]

TABLE V. Predicted InterPol signal levels during plasma current ramp. The expected interferometer two-pass phase shift and polarimeter two-pass Faraday rotation angle are calculated for the upper 27° chord of InterPol.

Time (s)	Plasma current (MA)	Interferometer phase shift $\Delta\phi$ (°)	Polarimeter Faraday rotation α (°)
0.5	0.63	22	0.01
1.0	0.87	48	0.02
3.0	2.78	214	0.16
5.0	4.74	340	0.31
8.0	7.45	1064	1.28
12.0	7.50	1091	1.29

In addition to the noise levels, one must consider the temporal resolution of the diagnostic if one wishes to measure fluctuations. It has been shown on previous systems that it is possible to obtain combined interferometer and polarimeter measurements at time resolutions of up to 500 kHz, which is more than sufficient for density feedback control.[22] In addition, polarimetry has been effectively used at up to 1 MHz.[15] This resolution has been sufficient to measure a variety of fluctuation modes via interferometry and polarimetry, including Alfvén eigenmodes (hundreds of kHz on current machines), quasi-coherent modes typical of EDA (enhanced D_α), H-mode plasmas (~100 kHz), and the weakly coherent mode (~300 kHz) typical of the I-mode.[15,22,39]

As one example of a feature that may be of interest on MQ1, one can estimate the frequency of toroidal Alfvén eigenmodes (TAEs) for these proposed machine parameters. This parameter is dependent on the device magnetic field and size, and thus is higher than the frequency that might be observed on a larger, lower magnetic field device. A typical frequency for a TAE is approximately[40]

$$f_A \approx \frac{v_A}{4\pi qR} \approx \frac{B_0}{4\pi qR\sqrt{\mu_0 n_i m_i}}, \tag{6}$$

where q is the safety factor, v_A is the Alfvén speed, and R is the machine major radius. Inserting the parameters for the MQ1 discharge described above gives an approximate TAE frequency of 400 kHz for a 50/50 DT mix. Assuming that a digitization system similar to that used in Ref. 15 is used for InterPol, it should be possible to resolve this signal and other features up to 1 MHz. It might be possible to in particular, tailor discharges to have lower frequency modes if these led to better measurements. Higher frequency modes [potentially including higher frequency AEs like EAEs (ellipticity-induced Alfvén eigenmodes) and (non-circular triangularity-induced) NAEs] will likely not be resolvable.

Finally, one must consider the spatial resolution of the diagnostic when making fluctuation measurements. Two aspects of the spatial resolution are of importance: the width of each beam and the spacing of the beam chords. As with the time resolution, only a very limited spatial resolution (really only one chord) is required for density feedback control. Current profile reconstruction may require somewhat higher resolution, especially in the outer core region where the bootstrap current is predicted to be significant, but again, this does not place particularly stringent constraints on the diagnostic geometry.

For fluctuations, a beam separation of ΔL gives a wavenumber resolution up to $k \sim 1/\Delta L$ for fluctuation measurements. Thus, a larger number of chords gives greater wavenumber resolution for the fluctuations and more information about the character of the measured fluctuations.[39] On the other hand, most previous interferometer and polarimeter fluctuation measurements were made with either one or two chords,[15,16,22] so fine wavenumber resolution is not required for useful fluctuation measurements.

In addition, the beam width w_0 of the interferometer and polarimeter lasers determines the minimum detectable fluctuation wavelength, since any fluctuation with a wavelength smaller than the beam width will be averaged out. The maximum measurable wavenumber is $k_{max} = 2/w_0$.[22] A similar CO_2 system on DIII-D has beam widths less than 8 mm,[22] allowing for measurements of fluctuations with wavenumbers up to 1.25 cm^{-1}. Another CO_2 system on Alcator C-Mod was able to measure wavenumbers up to 3.2 cm^{-1}.[39] With this level of resolution, it is possible to conduct comprehensive studies of density and magnetic field fluctuations within the available precision.[22,39]

VI. CONCLUSION

In conclusion, InterPol is a combined interferometer and polarimeter, which can measure both line-averaged density and internal poloidal magnetic field on a compact, high-field, high-density, net-energy tokamak, such as the MQ1 tokamak. Synthetic data testing and ray tracing suggest that InterPol will be able to make robust measurements with good resolution using a two-color CO_2 and QCL laser set. Poloidal polarimetry measurements with a reliable CO_2 laser are uniquely possible in a high-field, high-density machine such as MQ1. The noise levels, time resolution, and spatial resolution of InterPol are also sufficient to make fluctuation measurements of toroidal Alfvén eigenmodes and other phenomena on MQ1. InterPol represents the first design study of a combined interferometer polarimeter on a high-field, high-density, net-energy device.

AUTHOR'S CONTRIBUTIONS

A.J.C., L.M.M., and E.A.T. contributed equally to this work.

ACKNOWLEDGMENTS

The authors thank the Massachusetts Institute of Technology, Department of Nuclear Science and Engineering for its support of this research, as this work was conducted as part of a class. A. J. Creely is supported by the U.S. DoD and the Air Force Office of Scientific Research under the National Defense Science and Engineering Graduate (NDSEG) Fellowship, 32 CFR 168a. L. M. Milanese acknowledges support from the DoE under Grant No. DE-FG02-91ER54109. E. A. Tolman acknowledges support from the National Science Foundation Graduate Research Fellowship under Grant No. DGE-1122374.

REFERENCES

[1]J. Wesson, *Tokamaks*, International Series of Monographs on Physics, 4th ed. (Oxford University Press, 2011).
[2]F. Troyon, R. Gruber, H. Saurenmann, S. Semenzato, and S. Succi, "MHD-limits to plasma confinement," Plasma Phys. Controlled Fusion **26**(1A), 209 (1984).
[3]R. T. Mumgaard, M. Greenwald, J. P. Freidberg, S. M. Wolfe, Z. S. Hartwig, D. Brunner, B. N. Sorbom, and D. G. Whyte, "Scoping study for compact high-field superconducting net energy tokamaks," in *APS Division of Plasma Physics Meeting Abstracts* (APS Meeting Abstracts, 2016), Vol. 2016, p. BP10.029; available at https://ui.adsabs.harvard.edu/abs/2016APS..DPPB10029M.
[4]A. R. Polevoi, V. S. Mukhovatov, M. Shimada, S. Y. Medvedev, A. A. Ivanov, A. S. Kukushkin, and Y. Murakami, "ITER confinement and stability modelling," in Proceedings of Joint Conference of ITC-12 and APFA'01: Frontiers in Plasma Confinement and Related Engineering/Plasma Science (2003).
[5]B. Sorbom, J. Ball, T. Palmer, F. Mangiarotti, J. Sierchio, P. Bonoli, C. Kasten, D. Sutherland, H. Barnard, C. Haakonsen, J. Goh, C. Sung, and D. Whyte, "ARC: A compact, high-field, fusion nuclear science facility and demonstration power plant with demountable magnets," Fusion Eng. Des. **100**, 378 (2015).
[6]M. Greenwald, D. Whyte, P. Bonoli, Z. Hartwig, J. Irby, B. LaBombard, E. Marmar, J. Minervini, M. Takayasu, J. Terry, R. Vieira, A. White, S. Wukitch, D. Brunner, R. Mumgaard, and B. Sorbom, "The high-field path to practical fusion energy," PSFC Report No. RR-18-2 (2018).
[7]R. Mumgaard and SPARC Team, "SPARC and the high-field path," in 60th Annual Meeting of the APS Division of Plasma Physics (2018).
[8]E. Marmar, D. Brunner, M. Greenwald, Z. Hartwig, A. Hubbard, J. Irby, B. LaBombard, J. Minervini, R. Mumgaard, B. Sorbom, E. Tolman, D. Whyte, A. White, and S. Wukitch, "The high field tokamak path to fusion energy: C-Mod to SPARC to ARC," in 60th Annual Meeting of the APS Division of Plasma Physics (2018).
[9]A. White, S. Ballinger, A. Creely, S. Frank, A. Kuang, B. Linehan, W. McCarthy, L. Milanese, K. Montes, T. Mouratidis, J. Picard, P. Rodrigues Fernandez, A. Rosentha, A. Sandberg, F. Sciortino, R. Simpson, R. Tinguely, E. Tolman, M. Zhou, B. Sorbom, Z. Hartwig, and J. Irby, "Diagnostics for a SPARC-like, high-field, compact, net-energy tokamak," in *APS Division of Plasma Physics Meeting Abstracts* (APS Meeting Abstracts, 2018), p. UP11.707; available at https://ui.adsabs.harvard.edu/abs/2018APS..DPPU11070W.
[10]R. A. Tinguely, A. Rosenthal, R. Simpson, S. B. Ballinger, A. J. Creely, S. Frank, A. Q. Kuang, B. L. Linehan, W. McCarthy, L. M. Milanese, K. J. Montes, T. Mouratidis, J. F. Picard, P. Rodriguez-Fernandez, A. J. Sandberg, F. Sciortino, E. A. Tolman, M. Zhou, B. N. Sorbom, Z. S. Hartwig, and A. E. White, "Neutron diagnostics for the physics of a high-field, compact, Q1 tokamak," Fusion Eng. Des. **143**, 212 (2019).
[11]I. H. Hutchinson, *Principles of Plasma Diagnostics* (Cambridge University Press, 2002).
[12]V. V. Mirnov, W. X. Ding, D. L. Brower, M. A. V. Zeeland, and T. N. Carlstrom, "Finite electron temperature effects on interferometric and polarimetric measurements in fusion plasmas," Phys. Plasmas **14**(10), 102105 (2007).
[13]J. H. Irby, E. S. Marmar, E. Sevillano, and S. M. Wolfe, "Two-color interferometer system for Alcator C-MOD," Rev. Sci. Instrum. **59**(8), 1568 (1988).
[14]H. Soltwisch, "Current distribution measurement in a tokamak by FIR polarimetry (invited)," Rev. Sci. Instrum. **57**(8), 1939 (1986).
[15]W. F. Bergerson, P. Xu, J. H. Irby, D. L. Brower, W. X. Ding, and E. S. Marmar, "Far-infrared polarimetry diagnostic for measurement of internal magnetic field dynamics and fluctuations in the C-Mod tokamak (invited)," Rev. Sci. Instrum. **83**, 10E316 (2012).
[16]C. P. Kasten, J. H. Irby, R. Murray, A. E. White, and D. C. Pace, "A new interferometry-based electron density fluctuation diagnostic on Alcator C-Mod," Rev. Sci. Instrum. **83**, 10E301 (2012).
[17]S. C. Jardin, N. Pomphrey, and J. Delucia, "Dynamic modeling of transport and positional control of tokamaks," J. Comput. Phys. **66**, 481 (1986).
[18]B. Coppi and N. Sharky, "Model for particle transport in high-density plasmas," Nucl. Fusion **21**, 1363 (1981).
[19]W. M. Tang, "Microinstability-based model for anomalous thermal confinement in tokamaks," Nucl. Fusion **26**, 1605 (1986).
[20]M. A. V. Zeeland, T. N. Carlstrom, D. K. Finkenthal, R. L. Boivin, A. Colio, D. Du, A. Gattuso, F. Glass, C. M. Muscatello, R. O'Neill, M. Smiley, J. Vasquez, M. Watkins, D. L. Brower, J. Chen, W. X. Ding, D. Johnson, P. Mauzey, M. Perry, C. Watts, and R. Wood, "Tests of a two-color interferometer and polarimeter for ITER density measurements," Plasma Phys. Controlled Fusion **59**(12), 125005 (2017).
[21]H. Q. Liu, J. P. Qian, Y. X. Jie, W. X. Ding, D. L. Brower, Z. Y. Zou, W. M. Li, H. Lian, S. X. Wang, Y. Yang, L. Zeng, T. Lan, Y. Yao, L. Q. Hu, X. D. Zhang, and B. N. Wan, "Initial measurements of plasma current and electron density profiles using a polarimeter/interferometer (POINT) for long pulse operation in EAST," Rev. Sci. Instrum. **87**, 11D903 (2016).
[22]M. A. Van Zeeland, R. L. Boivin, D. L. Brower, T. N. Carlstrom, J. A. Chavez, W. X. Ding, R. Feder, D. Johnson, L. Lin, R. C. O'Neill, and C. Watts, "Conceptual design of the tangentially viewing combined interferometer-polarimeter for ITER density measurements," Rev. Sci. Instrum. **84**(4), 043501 (2013).
[23]J. P. Freidberg, F. J. Mangiarotti, and J. Minervini, "Designing a tokamak fusion reactor–How does plasma physics fit in?," Phys. Plasmas **22**(7), 070901 (2015).

[24]V. S. Voitsenya, A. J. Donné, A. F. Bardamid, A. I. Belyaeva, V. L. Berezhnyj, A. A. Galuza, C. Gil, V. G. Konovalov, M. Lipa, A. Malaquais, D. I. Naidenkova, V. I. Ryzhkov, B. Schunke, S. I. Solodovchenko, and A. N. Topkov, "Simulation of environment effects on retroreflectors in ITER," Rev. Sci. Instrum. **76**(8), 083502 (2005).
[25]D. Van Houtte, K. Okayama, and F. Sagot, "ITER operational availability and fluence objectives," Fusion Eng. Des. **86**, 680–683 (2011).
[26]T. N. Carlstrom, D. R. Ahlgren, and J. Crosbie, "Real–time, vibration–compensated CO_2 interferometer operation on the DIII–D tokamak," Rev. Sci. Instrum. **59**(7), 1063 (1988).
[27]P. Innocente, S. Martini, A. Canton, and L. Tasinato, "Upgrade of the RFX CO_2 interferometer using in-vessel optics for extended edge resolution," Rev. Sci. Instrum. **68**(1), 694 (1997).
[28]Y. Kawano, A. Nagashima, T. Hatae, and S. Gunji, "Dual CO_2 laser interferometer with a wavelength combination of 10.6 and 9.27 m for electron density measurement on large tokamaks," Rev. Sci. Instrum. **67**(4), 1520 (1996).
[29]D. R. Baker and S. Lee, "Dual laser interferometer for plasma density measurements on large tokamaks," Rev. Sci. Instrum. **49**(7), 919 (1978).
[30]A. J. H. Donne, A. Costley, R. Barnsley, H. Bindslev, R. Boivin, G. Conway, R. Fisher, R. Giannella, H. Hartfuss, M. von Hellermann, E. Hodgson, L. Ingesson, K. Itami, D. Johnson, Y. Kawano, T. Kondoh, A. Krasilnikov, Y. Kusama, A. Litnovsky, P. Lotte, P. Nielsen, T. Nishitani, F. Orsitto, B. Peterson, G. Razdobarin, J. Sanchez, M. Sasao, T. Sugie, G. Vayakis, V. Voitsenya, K. Vukolov, C. Walker, K. Young, and ITPA Topical Group on Diagnostics, "Chapter 7: Diagnostics," Nucl. Fusion **47**, S337 (2007).
[31]K. Kawahata, A. Ejiri, K. Tanaka, Y. Ito, and S. Okajima, "Design and construction of a far infrared laser interferometer for the LHD," Fusion Eng. Des. **34–35**, 393 (1997).
[32]A. Mlynek, G. Schramm, H. Eixenberger, G. Sips, K. McCormick, M. Zilker, K. Behler, J. Eheberg, and ASDEX Upgrade Team, "Design of a digital multiradian phase detector and its application in fusion plasma interferometry," Rev. Sci. Instrum. **81**, 033507 (2010).
[33]A. Mlynek, L. Casali, O. Ford, H. Eixenberger, and ASDEX Upgrade Team, "Fringe jump analysis and implementation of polarimetry on the ASDEX Upgrade DCN interferometer," Rev. Sci. Instrum. **85**, 11D408 (2014).
[34]G. Braithwaite, N. Gottardi, G. Magyar, J. R. J. O'Rourke, and D. Veron, "JET polari-interferometer," Rev. Sci. Instrum. **60**, 2825 (1989).
[35]K. Kawahata, T. Akiyama, K. Tanaka, S. Okajima, and K. Nakayama, "Recent progress in two-color laser diagnostics," J. Phys. **227**, 012022 (2010).
[36]K. Kawahata, T. Akiyama, K. Tanaka, K. Nakayama, and S. Okajima, "Progress in development of two color laser diagnostics for the ITER poloidal polarimeter," J. Instrum. **7**(2), C02002 (2012).
[37]J. Chen, G. Zhuang, Q. Li, Y. Liu, L. Gao, Y. N. Zhou, X. Jian, C. Y. Xiong, Z. J. Wang, D. L. Brower, and W. X. Ding, "High resolution polarimeter-interferometer system for fast equilibrium dynamics and MHD instability studies on joint-TEXT tokamak (invited)," Rev. Sci. Instrum. **85**, 11D303 (2014).
[38]M. A. Van Zeeland, R. L. Boivin, T. N. Carlstrom, and T. M. Deterly, "CO_2 laser polarimeter for Faraday rotation measurements in the DIII-D tokamak," Rev. Sci. Instrum. **79**, 10E719 (2008).
[39]C. P. Kasten, A. E. White, and J. H. Irby, "A new fast two-color interferometer at Alcator C-Mod for turbulence measurements and comparison with phase contrast imaging," Phys. Plasmas **21**(4), 042305 (2014).
[40]W. W. Heidbrink, "Basic physics of Alfvén instabilities driven by energetic particles in toroidally confined plasmas," Phys. Plasmas **15**(5), 055501 (2008).